Journal of Crystal Growth 311 (2009) 1166–1177

Contents lists available at ScienceDirect

Journal of Crystal Growth

journal homepage: www.elsevier.com/locate/jcrysgro

Reconstruction of time-dependent concentration gradients around a KDP crystal growing from its aqueous solution

Atul Srivastava *,[1], Dhruv Singh, K. Muralidhar

Department of Mechanical Engineering, Indian Institute of Technology, Kanpur 208016, India

ARTICLE INFO

Article history:
Received 23 April 2008
Received in revised form
20 November 2008
Accepted 1 December 2008
Communicated by J. de Yoreo
Available online 7 December 2008

PACS:
47.55.P–
81.10.Dn
77.84.Fa
42.79.Mt
81.70.Tx

Keywords:
A1. Convection
A1. Mass transfer
A1. Optical tomography
A1. Time-dependent fluid flows
A2. Growth from solutions
B1. KDP

ABSTRACT

Reconstruction of the steady three-dimensional concentration field from path-integrated two-dimensional data has been studied by the authors earlier. The extension of this approach to reconstruct three-dimensional unsteady concentration gradient field around a KDP crystal growing from its aqueous solution is examined in the present work. The experiments reported in the present work have been carried out in the mixed convection regime where inertial as well as buoyancy effects are significant. The crystal size is large enough to induce a time-dependent movement of convection currents in the growth chamber. Laser schlieren is used as the measurement technique for mapping the concentration gradients around the crystal. Projection data is in the form of a time sequence of schlieren images over an angular span of 0–360°. Images are recorded by rotating the growing crystal while the growth chamber is kept fixed. The time sequence recorded for one projection is uncorrelated to the next, creating an asynchronous data set. The technique proposed herein is an application of proper orthogonal decomposition to the image sequence. The method decouples the spatial and temporal components of the measured time-dependent data. The spatial modes, in turn, are ordered across all projections, thus facilitating three-dimensional reconstruction over the entire physical domain. The algorithm proposed integrates principles of tomography with proper orthogonal decomposition. It has been validated with simulated as well as experimental data. The results show that the first few modes contain much of the information of the time-dependent growth process. The differences in the nature of temporal fluctuations of the concentration gradient field in regions close to the growing crystal against those in the bulk are clearly revealed. The concentration gradient field is found to be purely unsteady near the crystal–solution interface, whereas the level of temporal fluctuations decreases as one moves towards the bulk of the solution. The reconstructed POD modes reveal an overall axisymmetry of the concentration gradients field in the growth chamber while a slight loss of symmetry was revealed in the vicinity of the growing crystal.

1. Introduction

Good quality crystals of various sizes find applications in many technologically important areas ranging from lasers to biomedical applications. Forming a crystal from a supersaturated aqueous solution is a popular growth technique. The process is accompanied by a three-dimensional time-varying concentration gradient field in the vicinity of the crystal. In the presence of gravity, the gradients in the density of the solution are responsible for the evolution of buoyancy-driven convection currents. These are oscillatory and, in general, time-dependent and drastically modify the concentration field and its gradients along the crystal–solution interface. The growth rates and defect structures of the growing crystal (such as step bunches and solution inclusions) are functions of the coupled mechanisms of time-dependent fluid flows and mass transport in the growth chamber. These mechanisms are often detrimental to the quality of the growing crystal. Hence, mapping of the three-dimensional concentration field and its gradients in the vicinity of the growing crystal are required to establish appropriate conditions for growing large defect-free crystals [1–3]. Growth from an aqueous solution is particularly amenable to optical visualization, since the solution is transparent. It is possible to generate images of the convective field by exploiting changes in the refractive index that accompany changes in the density of the medium. Optical techniques are ideal for mapping the properties of the solution during a crystal growth experiment because they are non-intrusive and inertia-free [4–7].

In a crystal growth experiment, the projection data for various view angles can be recorded either by turning the crystal growth chamber or the source–detector combination. In these configurations,

*Corresponding author. Tel.: +81 22 795 5903; fax: +81 22 795 6661.
E-mail addresses: atulsr@ganko.tohoku.ac.jp, atulsr@rrcat.gov.in (A. Srivastava).
[1] Present address: Department of Earth and Planetary Materials Science, Graduate School of Science, Tohoku University, Aramaki, Aoba, 980-8578 Sendai, Japan.

0022-0248/$ - see front matter © 2008 Elsevier B.V. All rights reserved.
doi:10.1016/j.jcrysgro.2008.12.001

a finite time elapses while moving from one view angle to the other and hence the projection data recorded is asynchronous in time if the temporal changes in the concentration gradients field are faster than the speed at which the projection data is recorded from different view angles. When the field of interest varies with respect to time, the projection data from all view angles should be correlated for principles of tomography to apply. Accordingly, one needs to record information simultaneously from all the view angles. However, this method of simultaneously recording the projection data requires multiple source–detector combinations. The technique of proper orthogonal decomposition (POD) applied to the projection sequence offers a simpler alternative to handle asynchronous projection data and is the subject of the present study.

Importance of the reconstruction of three-dimensional temperature and/or concentration field and its gradients in a crystal growth process has been emphasized in the literature by various researchers over the last few decades. However, the literature on the application of tomographic algorithms for the determination of the three-dimensional concentration field from optical images shows that predominantly the steady state alone has been considered. In an earlier work, Bedarida et al. [8] proposed multidirectional holographic interferometric tomography technique to reconstruct the three-dimensional concentration field on horizontal planes above a sodium chlorate crystal growing from its aqueous solution. Notcovich et al. [9] investigated the three-dimensional temperature field around heavy ice growing from supercooled heavy water using interferometric tomography. Srivastava et al. [10] determined the three-dimensional steady concentration field around a KDP crystal growing from its aqueous solution using the laser schlieren technique. Masayuki et al. [11] employed a Mach–Zehnder interferometer for the measurement of two-dimensional concentration gradients around a KDP crystal growing from its aqueous solution. In the context of imaging an unsteady concentration field, Yokoyama et al. [12] presented a method to visualize the time-dependent concentration field around a growing crystal in solution. However, the subject of three-dimensional analysis of a time-dependent concentration field around a growing crystal has not been addressed yet. The present work is concerned with the application of the POD technique jointly with convolution back projection (CBP) for the spatial reconstruction of time-varying concentration gradient fields around a KDP crystal growing from its aqueous solution. The specific goals of the present study are (a) introduction and application of POD-based inversion scheme for the reconstruction of time-dependent concentration gradient field in a crystal growth process, (b) validation of the proposed scheme against numerical and experimental data and (c) reconstruction of concentration gradient field at select horizontal planes above the growing crystal. Reconstructions have been performed both near the crystal–solution interface as well as in the regions away from the growing crystal to examine the temporal fluctuations in the concentration gradient field. These, in turn, affect the rate of solute transport from the solution to the growing crystal surfaces and hence the growth rates of various crystal faces.

2. Proposed reconstruction scheme

The central idea behind the proposed scheme is the following: by definition, the optical projections of a given flow field in the schlieren arrangement are the line integrals of the concentration gradient field along the viewing direction. In POD, the gradient field is decomposed into a product of two functions that individually depend on space and time. The path integrals are only defined in space. Hence, the time-dependent function must remain unaltered even though projections are recorded at different time instants. The aim of completely decoupling the temporal and spatial components of the field of interest is thus accomplished using proper orthogonal decomposition. The integration of proper orthogonal decomposition with CBP presents a novel approach to reconstruct the unsteady field of interest from its asynchronous projection data.

2.1. Proper orthogonal decomposition

The proper orthogonal decomposition method provides a methodology for extracting the proper orthogonal modes from experimental or simulated data. These proper orthogonal modes contain information about the dominant features of the process under study and carry the greatest energy on an average. The modes are used to construct a set of basis functions (for a continuous system) or basis vectors (in the case of discrete systems). The basis functions or basis vectors form the reduced order model of the physical phenomenon under investigation. Though well established in image processing and pattern recognition [13,14], its application towards the investigation of time-dependent transport phenomena associated with a crystal growth process is completely new. The technique has been widely applied to unsteady computational fluid dynamics formulations [15,16]. In the context of crystal growth, POD has been applied as an optimal control problem for fluid flows in a horizontal chemical vapor deposition reactor [17].

The basic POD procedure can be summarized briefly as follows: an ensemble of images collected over a period of time can be represented by the symbol $\psi(x,t)$ and approximated as a finite sum in the variables separated form

$$\psi = \psi(x,t) \approx \sum_{k=1}^{N} \alpha_k(t)\mu_k v_k(x) \approx \sum_{k=1}^{N} u_k(t)v_k(x) \tag{1}$$

The approximation becomes exact as N approaches infinity. In Eq. (1), the symbol t is the time index when the image is recorded and x is the pixel location in 1 or 2 dimensions. The image definition for the present study is in terms of a set of intensity values at various pixel locations recorded at a time instant t. However, the representation of ψ in terms of the basis functions is not unique. Several choices of $v_k(x)$ are possible and for each choice the sequence of time-dependent functions $u_k(t)$ is unique. Proper orthogonal decomposition is concerned with finding the best possible choice of the functions $v_k(x)$ for a collection of images $\psi(x,t)$. The basis functions are taken to be orthonormal so that the determination of the coefficient function $u_k(t)$ for a given k will depend only on $v_k(x)$ and not on the other v's. Orthonormality requires

$$\int_x v_k(x)v_l(x)dx = \{1 \text{ if } k = l \text{ and } 0 \text{ otherwise} \tag{2}$$

The time-dependent part can then be obtained as:

$$u_k(t) = \int_x \psi(x,t)v_k(x)dx$$

The determination of the coefficient function $u_k(t)$ for a given k depends only on $v_k(x)$ and not on the other v's. The orthonormal property of Eq. (2) is useful while selecting functions $v_k(x)$ only in the limit of N approaching infinity. If N is finite but reasonably large, we choose the basis functions $v_k(x)$ in such a way that the approximation for each N is the best possible in a least squares sense [13]. In the present work, POD modes have been determined using routines available in MATLAB. Ordered, orthonormal functions $v_k(x)$ are the proper orthogonal modes or the basis

functions of $\psi(x,t)$. With these functions computed, Eq. (1) is the proper orthogonal decomposition of $\psi(x,t)$.

2.2. Convolution back projection

Reconstruction of a three-dimensional field from two-dimensional projections has been accomplished in the present work using the convolution back projection algorithm (CBP). The algorithm works with the one dimensional projection data of each plane of the three-dimensional field. The use of CBP in the present work has been preferred because of its significant advantages such as non-iterative character, availability of analytical results on convergence and established error estimates [18,19]. Here, the reconstructed function $f(r,\phi)$, is evaluated by the integration formula [20,21]:

$$f(r,\phi) = \int_0^{\pi} \int_{-D/2}^{D/2} p((s'-s);\theta) q(s) ds d\theta \tag{3}$$

where

$$q(s) = \int_{-R_c}^{R_c} |R| W(R) \exp(i2\pi R s) dR$$

Here, $p(s;\theta)$ is the projection data and s is the perpendicular distance of the data ray from the center of the object. In addition, θ denotes the source–detector line with respect to a fixed axis (and hence the view angle), D is the diameter of the growth chamber, and s' is the s-value of the data ray passing through the point (r,ϕ). The symbol R is the Fourier frequency, $q(s)$ is the convolving function of Eq. (3), and W(R), is the filter function. The filter function vanishes outside the interval $[-R_c,+R_c]$ and is an even function of R. Here, R_c is the Fourier cut-off frequency and is taken to be $\frac{1}{2}\Delta s$, Δs being the ray spacing. The reconstruction obtained is specific to the choice of the filter function [19–21]. A Hamming filter h54 has been used in the present study. The experience of the authors with CBP in the context of schlieren imaging can be seen in Ref. [10].

2.3. Combined POD–CBP algorithm

The approach integrating tomography and proper orthogonal decomposition technique for the three-dimensional reconstruction of the unsteady concentration gradient field is described in the present section. The projection data in the form of time-dependent schlieren images has been recorded for a given position of the laser-camera axis with respect to the test apparatus. The growth chamber has been kept fixed and the projection data for various view angles have been extracted from the sequence of schlieren images of the convective field around the rotating crystal. A time series of images in real time over a period of around 24 s was experimentally recorded. Since the crystal was rotated at a rate of 15 rpm, the projection data at six separate time instants could be extracted from the recorded time sequence for a given view angle in the range of 0–360°. Moreover, since the light intensity scales linearly with the concentration gradient, numerical calculations can be performed directly with light intensity. The final results are presented in dimensionless form. Reconstructions are performed at horizontal planes above the crystal; hence the modes of the time sequence of light intensity values along a row of the schlieren image constitute the data set for tomography.

The experimental data is now processed as per the following algorithm:

1. Start with the image data for a given view angle.
2. Select a horizontal plane above the growing crystal from the schlieren image where the reconstruction is to be performed.
3. For the selected plane, form the POD data matrix. For a given time instant, express the intensity values as the column of the matrix. Similarly intensity data for other time instants form the remaining columns.
4. Subtract out the average of every column; modal analysis is performed for the mean-removed data.
5. For the rectangular matrix thus obtained, determine the POD basis vectors and the corresponding time components.
6. Repeat steps 1–5 for all view angles. Modes of each projection (between 0° and 180°) have now been obtained by considering all the time instants.
7. Use a tomography algorithm (CBP, in the present study) to convert the modes of projection data into the 2-D modes of concentration gradient over selected horizontal plane above the crystal.
8. Repeat step 7 for as many modes as are significant.
9. Determine the reconstructed time-dependent concentration gradient field by multiplying the 2-D spatial modes by the respective time components available at step 5.

It is to be mentioned here that in the present work the proposed reconstruction scheme has been employed for the determination of the three-dimensional distribution of concentration gradients rather than the concentration itself. This is important because during solution growth, the growth rates of various faces of the crystal are intricately linked with the spatial and temporal distributions of these gradients in the growth chamber. However, the POD-based technique can be easily extended for the determination of the three-dimensional concentration field itself. Here, instead of starting with the time sequence of light intensity values in a schlieren image directly (Step 1 of the algorithm), one first calculates the integrated (ray-averaged) concentration field for a given view angle. Similarly, the concentration fields for all the view angles are calculated independently from the recorded schlieren images. The steps involved in determining the ray-averaged concentration field from the schlieren images have been demonstrated earlier by the authors elsewhere [10,22,23]. A detailed procedure for analyzing schlieren images can also be found in the literature [4]. The ray-averaged concentration field thus obtained for each view angle and for a given time instant now replaces the original intensity values in a schlieren image as the input to the algorithm described above. One follows the remaining steps of the algorithm to determine the instantaneous three-dimensional concentration field in the growth chamber.

It is important to mention here that the reconstruction scheme proposed here is not restricted to image the growth of crystals from their aqueous solution. It can efficiently be employed to investigate the three-dimensional temperature and concentration fields in other crystal growth processes as well, e.g. melt growth. One such area of interest is the understanding of three-dimensional temperature distribution during the formation of chondrules (silicate spheres, a few mm in diameter). The temperature distribution inside silicate melts severely affects the process of crystallization. Since the process of crystallization is very rapid [24], the changes in the temperature field inside the silicate spheres are strongly time-dependent. The reconstruction scheme proposed in the present work avoids the requirement of multiple source–detector combinations and high speed cameras for such applications in order to capture the transients of the temperature field and presents an efficient method for the reconstruction of three-dimensional temperature distribution.

3. Validation of POD against experimental data

The present section discusses the experimental validation of reduced order reconstruction using the proper orthogonal

decomposition technique. The physical problem considered is buoyancy-driven convection in a fluid medium that is confined in a horizontal differentially heated rectangular cavity. The experimental set up is schematically shown in Fig. 1(a). The working fluid is air. The horizontal surfaces of the cavity provide a temperature difference for initiating convection in the fluid, the vertical sides of the cavity being thermally insulated. The temperature difference across the cavity is 10 °C. Projection data in the form of two-dimensional images have been recorded using a Mach–Zehnder interferometer [3,4]. A continuous time sequence of images was recorded in the form of a movie at video rates (25 frames per second). An ensemble of 10 consecutive images constituted the basic data set for POD analysis. The images of this ensemble were converted to a two-dimensional matrix, each column containing intensity data of a snap shot, the number of images being equal to the number of columns. The POD modes are those of this rectangular matrix.

Fig. 1(b) shows the POD modes of the interferograms for a particular ensemble of images recorded. One of the instantaneous original images from the time sequence has also been shown in the figure. The variation of energy of each of the modes with respect to the eigen index is shown in Fig. 1(c). It is seen that the 100% of the energy scale is reached in around eight modes. Thus, modes of higher order (>8) can be dropped from further consideration.

Fig. 2 shows a comparison of the reconstructed interferogram with eight POD modes with the corresponding instantaneous original images of the ensemble. The difference between intensity values of the reconstructed and the original images for each pixel (error/pixel) is displayed in the form of an image in the third column. It is seen that the approximations match quite closely with the original images. The maximum deviation is of the order of 10^{-15} and can be attributed to the error involved in truncating beyond the 8th POD mode.

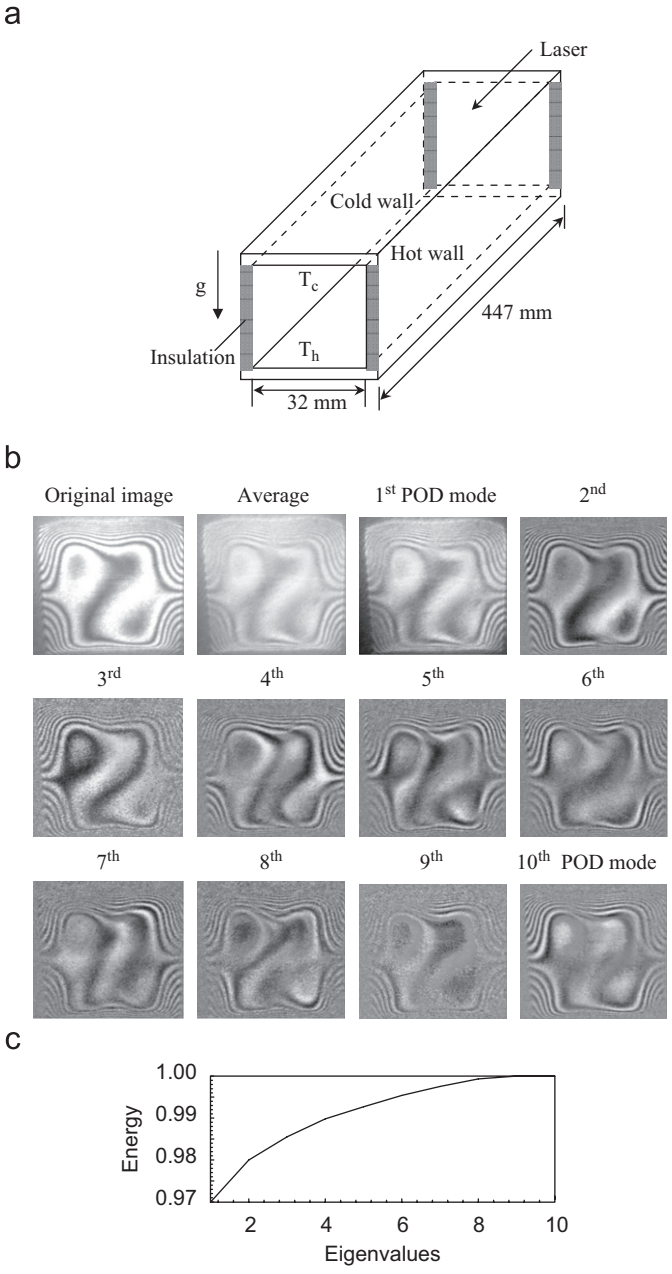

Fig. 1. (a) Schematic drawing of rectangular cavity setup, (b) POD basis vectors of an interferometric image sequence of convective field in a differentially heated rectangular cavity. One of the original images from the ensemble and the average image has also been shown and (c) variation of energies with respect to Eigen indices.

4. Validation of POD and tomographic reconstruction with respect to analytical data

The reconstruction algorithm of Section 2.3 has been validated against a numerically simulated time-dependent field. This field is an axially symmetric Gaussian distribution of light intensity varying sinusoidally in time and is expressed as:

$$C(x,y,t) = R_0^{(0.5+0.25\sin(2\pi t/T))} - (x^2+y^2)^{(0.5+0.25\sin(2\pi(t/T))/2)} \quad (4)$$

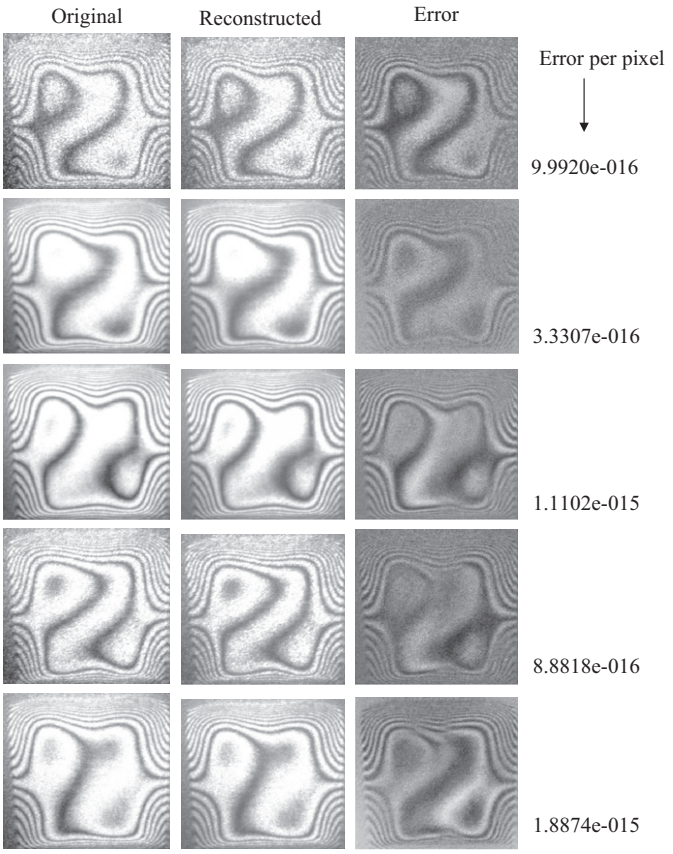

Fig. 2. Comparison of the reconstructed interferometric images (column 2) with the original images (column 1) of the ensemble. Deviations of the intensity values between original and the reconstructed images have also been shown in the form of error images (column 3).

Here, R_0 is the radius of the physical domain while x and y are the coordinates of any point in the plane as measured from the center. The time period of the cycle is denoted as T.

Starting with the analytical form of the dependent variable given by Eq. (4), projection data as line integrals are calculated by numerical integration along the viewing direction. Since the field is axisymmetric, data sets of all projections are identical.

The zeroth order POD mode is just the time-average of the function C evaluated over the time period. Higher order POD modes, are displayed as two-dimensional images in Fig. 3(a). The variation of the energy content of each mode with respect to eigenvalue index is shown in Fig. 3(b). For the present example Eq. (4), it is seen that the first POD mode already contains most of the energy while other modes have a negligible contribution. The field given by Eq. (4) is reconstructed using the algorithm of Section 2.3. The accuracy of reconstruction is estimated in terms of the percentage RMS error between the reconstructed and the exact, namely Eq. (4), for each time instant. Fig. 3(c) shows the variation of the RMS error with respect to time for 18 and 90 projections. Errors are a maximum of 26% for 18 projections, while they reduce to 2.5% for 90 projections. In a steady state context, errors are slightly smaller, as discussed in Ref. [10].

5. Reconstruction of the unsteady concentration gradient field in crystal growth

The present section describes the application of the combined POD–CBP algorithm for the reconstruction of the unsteady concentration gradient field above a KDP crystal growing from its aqueous solution. The growth experiment has been performed in the mixed convection regime. The crystal size is large enough to induce a time-dependent movement of the convection currents in the apparatus. An additional motion in the form of crystal rotation at 15 RPM is also imparted. The growth process is initiated by introducing a spontaneously crystallized KDP seed into its super-saturated solution. Slow cooling of the solution results in the deposition of excess salt from the solution to the crystal faces. The

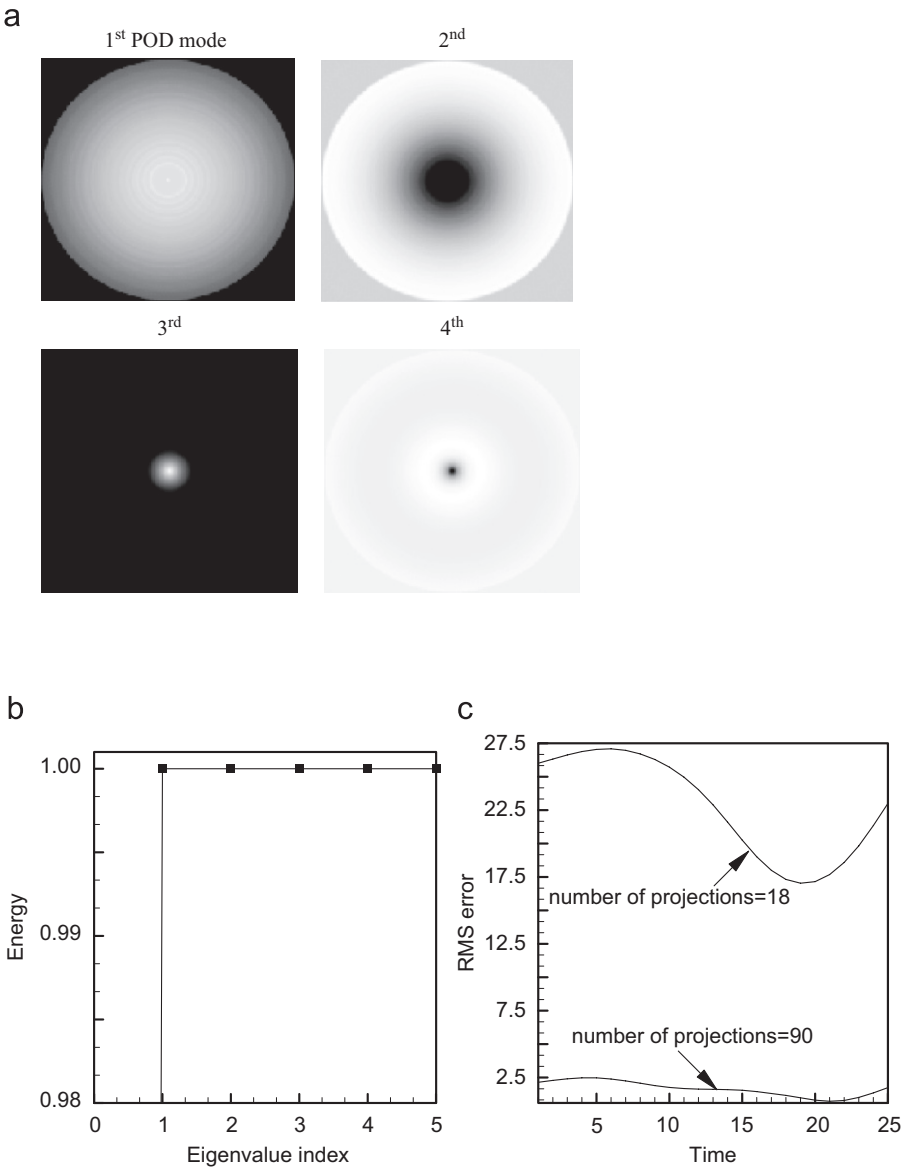

Fig. 3. (a) POD modes for an analytically simulated field, (b) variation of energies of the reconstructed modes with respect to Eigen mode indices and (c) percentage RMS error in reconstruction as a function of time count for 18 and 90 projections.

reduction in the solutal concentration around the crystal leads to the appearance of concentration gradients in its vicinity. These gradients are responsible for the movement of the fluid particles in the growth chamber. The onset of fluid motion is determined by the relative magnitudes of the driving buoyancy force and the resistive viscous force. When the crystal size is small, the fluid movement around the growing crystal is symmetric. Since the solution is cooled at a very slow rate, the growth process is steady. With an increase in crystal size, the driving potential responsible for the fluid motion in the growth chamber increases in magnitude and the convection currents tend to become vigorous and time-dependent.[2] To understand the resulting distribution of the salt around the crystal, it is important to analyze the time-dependent three-dimensional distribution of concentration gradients field in the growth chamber.

5.1. Apparatus and Instrumentation

The crystal growth experiments have been performed in a glass chamber schematically shown in Fig. 4(a). It comprises a beaker that holds the KDP solution and has a diameter of 16.5 and 23 cm height. The temperature of the KDP solution in the inner beaker is controlled by thermostated water circulated in the outer chamber. The outer chamber is octagonal in plan and is made of Plexiglas. It ensures a large enough volume for the circulating thermostated water to keep the KDP solution at the required temperature level over a period of time. The temperature of the circulating water in the outer chamber is controlled by four symmetrically located heating elements whose electrical input is regulated by a programmable temperature controller (*Eurotherm*). A k-type thermocouple wire fixed to the outer surface of the growth chamber (inner beaker) provides the feedback to the controller. Uniformity of temperature within the solution is ascertained by recording temperatures at various locations using 26-gauge k-type thermocouples. For visualization of the concentration gradient field by the schlieren technique, circular optical windows (BK-7, 40 mm diameter, 5 mm thickness, $\lambda/4$) are fixed on the glass beaker at its opposite ends.

A Z-type monochrome schlieren technique (Fig. 4(b)) is employed for the visualization of the concentration gradients field in the growth chamber [25]. From the gradient field and knowledge of concentration far away from the crystal, solute concentration can be determined everywhere in the field of view. The schlieren system has concave mirrors, flat mirrors, knife-edge and a laser. The growth cell under study is placed between the two concave mirrors as shown in the figure. The concave mirrors used in the present work are of 1.30 m focal length each and 200 mm diameter. The knife-edge is placed at the focal length of the second concave mirror. It is positioned to cut off a part of the light focused on it so that, in the absence of any optical disturbance, the illumination on the screen is uniformly reduced. The knife-edge is oriented perpendicular to the direction in which the density gradients in the aqueous solution are to be recorded. In addition, the field of view includes the undisturbed solution away from the crystal, where the solutal concentration is a known quantity. In the present study, the gradients are expected to be predominantly in the vertical direction parallel to the gravity vector and the knife-edge has been kept horizontal. The schlieren

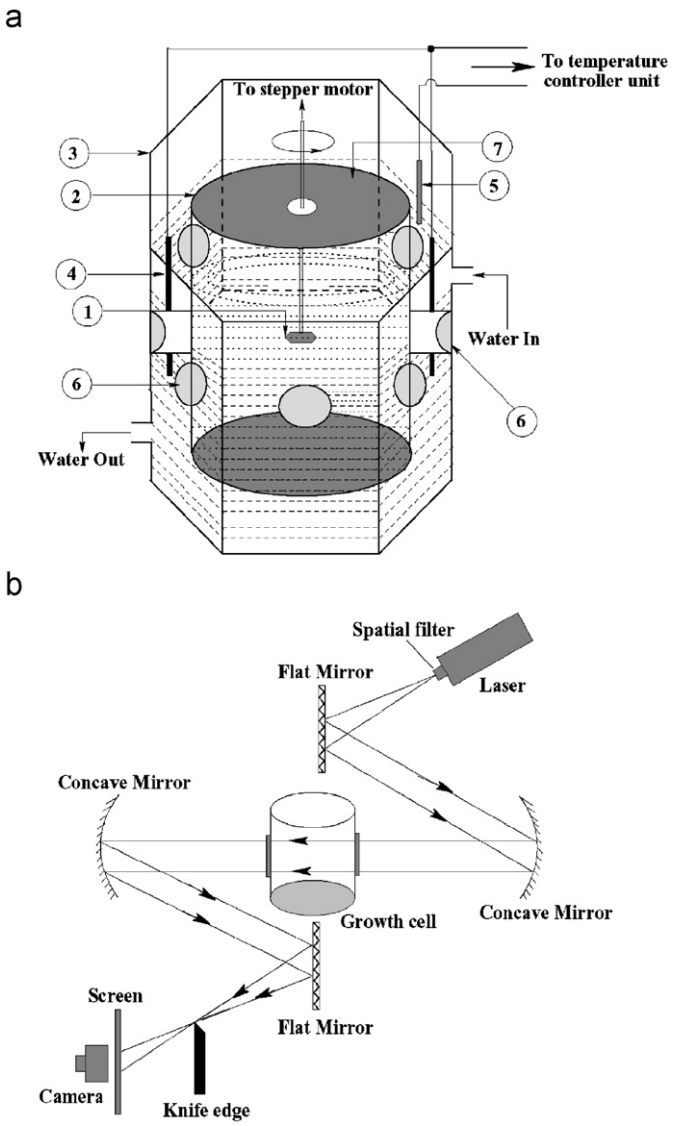

Fig. 4. Schematic diagram of Four-view crystal growth chamber (a) and Z-type laser schlieren set up (b). (1) Growing crystal, (2) growth chamber, (3) outer chamber, (4) heating element, (5) thermocouple, (6) optical window and (7) covering lid.

image is a line integral of the local concentration gradient field in the viewing direction [4]. Hence, it constitutes the projection data from which the local gradients are to be determined. Since the crystal is imparted rotation, a time sequence of schlieren images recorded rapidly yields both the time series of images for a given projection angle and projection data for a large number of view angles within 0° and 180°. A typical time sequence of schlieren images for a complete cycle (between 0° and 180°, in an interval of 45°) is shown in Fig. 5.

For optical measurements, a continuous wave helium–neon laser (*Spectra Physics*, 35 mW) has been employed as the laser source. A monochrome CCD camera (*Sony*) of spatial resolution of 768×574 pixels was used to record the convective field in the form of two-dimensional images. The camera was interfaced with a personal computer (*HCL*, 256 MB RAM, 866 MHz) through an 8-bit frame grabber card. Light intensity levels were digitized over the range 0 (dark)–255 (bright). Image acquisition was at video rates namely 25 frames/s. The temporal information of the concentration gradient field has been recorded in the experiments

[2] The relative strengths of buoyancy and viscous forces can be defined in terms of a non-dimensional parameter, the Rayleigh number, expressed as $Ra=((g\beta(\Delta C)d^3)/\nu\alpha)$, where d is the crystal diameter, g is the acceleration due to gravity, β is the volumetric coefficient of expansion, ν is kinematic viscosity, α is the thermal diffusivity of the fluid and ΔC is the degree of supersaturation of the solution at a given time instant. For the experiments reported in the present work, the Rayleigh number based on the crystal diameter was calculated to be in excess of 10^6.

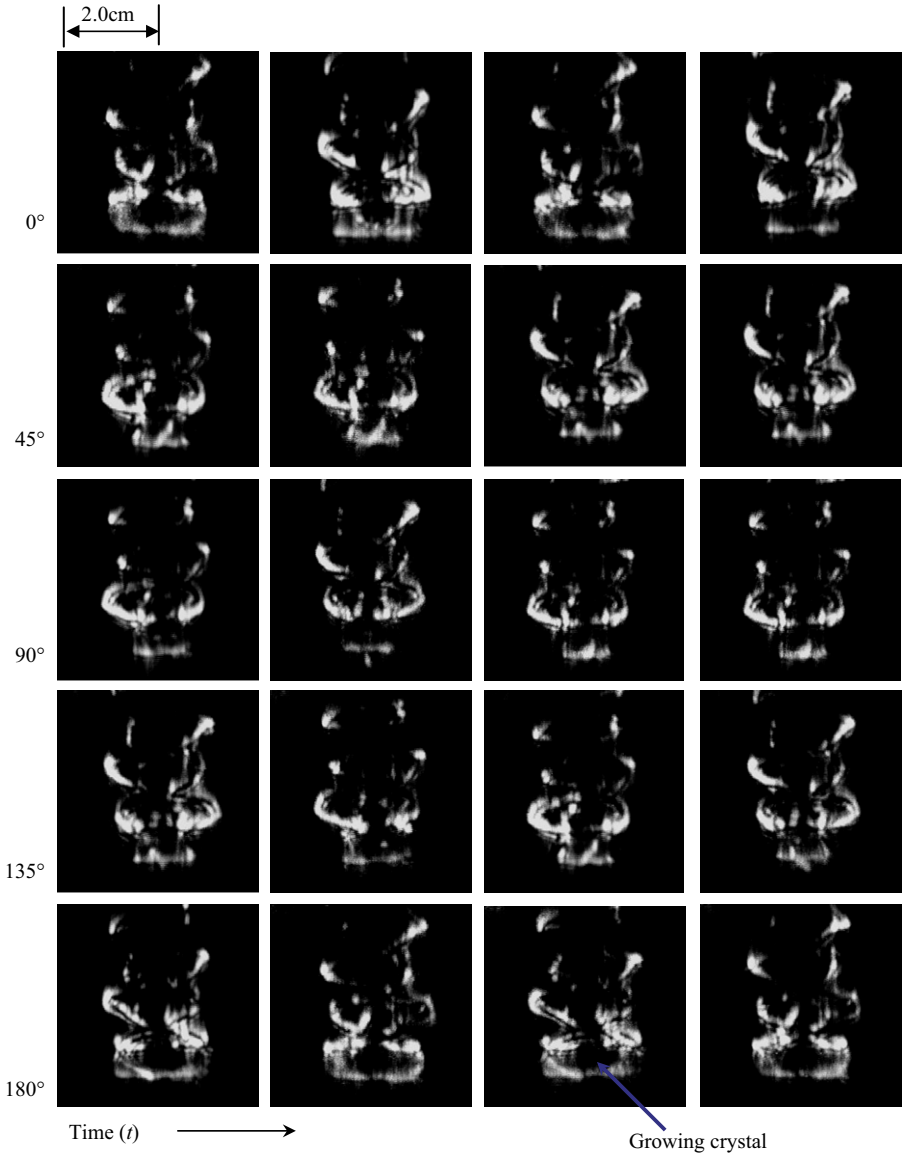

Fig. 5. Schlieren images of the time-dependent convective field around a KDP crystal growing from its aqueous solution at four different time instants. Images over a full cycle (0–180°, in an interval of 45°) have been shown. Bright regions are zones of high concentration gradients. The dark region away from the crystal shows the undisturbed supersaturated solution.

by collecting time series of schlieren images in real time over a period of around 24 s. Since the growing crystal is imparted rotation at a rate of 15 rpm (one rotation in 4 s), schlieren images at six different time instants could be experimentally recorded for a given projection angle (between 0 and 180°). Furthermore, since the rate of crystal rotation is kept constant, the temporal information at intermediate time instants has been generated by interpolating the consecutively recorded intensity values (equally spaced with an interval of 4 s). A time series with 20 entries for a given view angle is thus available for the POD analysis. The experimental apparatus and laser instrumentation utilized for the present work are similar to those reported by the authors earlier [10]. The analysis of schlieren images is discussed in various Refs. [3,4,10,22,23,25].

6. Results

The reconstruction results using the proposed inversion scheme for determining the time-dependent concentration gradient field over planes above the growing crystal have been presented in this section. A set of schlieren images as a function of time and view angles employed in the analysis is shown in Fig. 5. Results have been presented in the form of two-dimensional modal images of the time-dependent concentration gradient field obtained using the integrated approach of proper orthogonal decomposition and CBP. The symmetry of the gradient field in the growth chamber has been discussed in qualitative terms on the basis of the two-dimensional modal images. Further, the approach has been extended to demonstrate the reconstruction of the time-dependent concentration gradient field in quantitative terms by using the time components available after POD analysis (Section 2.3).

Image formation in a schlieren system is due to the deflection of the light beam in a variable refractive index field toward the region of higher refractive index. In the context of crystal growth experiments reported in the present study, the deposition of solute onto the crystal faces leads to the formation of solutal concentration gradients in the growth chamber. The intensity contrast, as observed in the schlieren images shown in Fig. 5, is

related to a change in the solute concentration around the growing crystal. It creates a jump in the refractive index and deflects the light beam into the region of relatively large concentration gradients. As defined by the bright intensity regions in the images, the combined effect of buoyancy and rotational forces govern the overall orientation and movement of the convection currents around the crystal. The effective movement of the fluid particles is along a helical path as seen in the schlieren images in Fig. 5.

It is to be noted here that the images recorded by the schlieren apparatus yield the line-integrated values of concentration gradients. The relationship between light intensity and the solutal gradient is linear. Hence, the resultant intensity distribution in the images yields a qualitative measure of the strength of concentration gradients prevailing in the growth chamber. Normalized gray scale values of light intensity (in the range of 0–255) of the recorded schlieren images have been utilized for generating concentration gradient field data at selected horizontal planes above the growing crystal. A time series of over 20 images was used in the analysis, though it was sufficient to employ less than 20 POD modes. Reconstruction has been performed with a total of 90 projections.

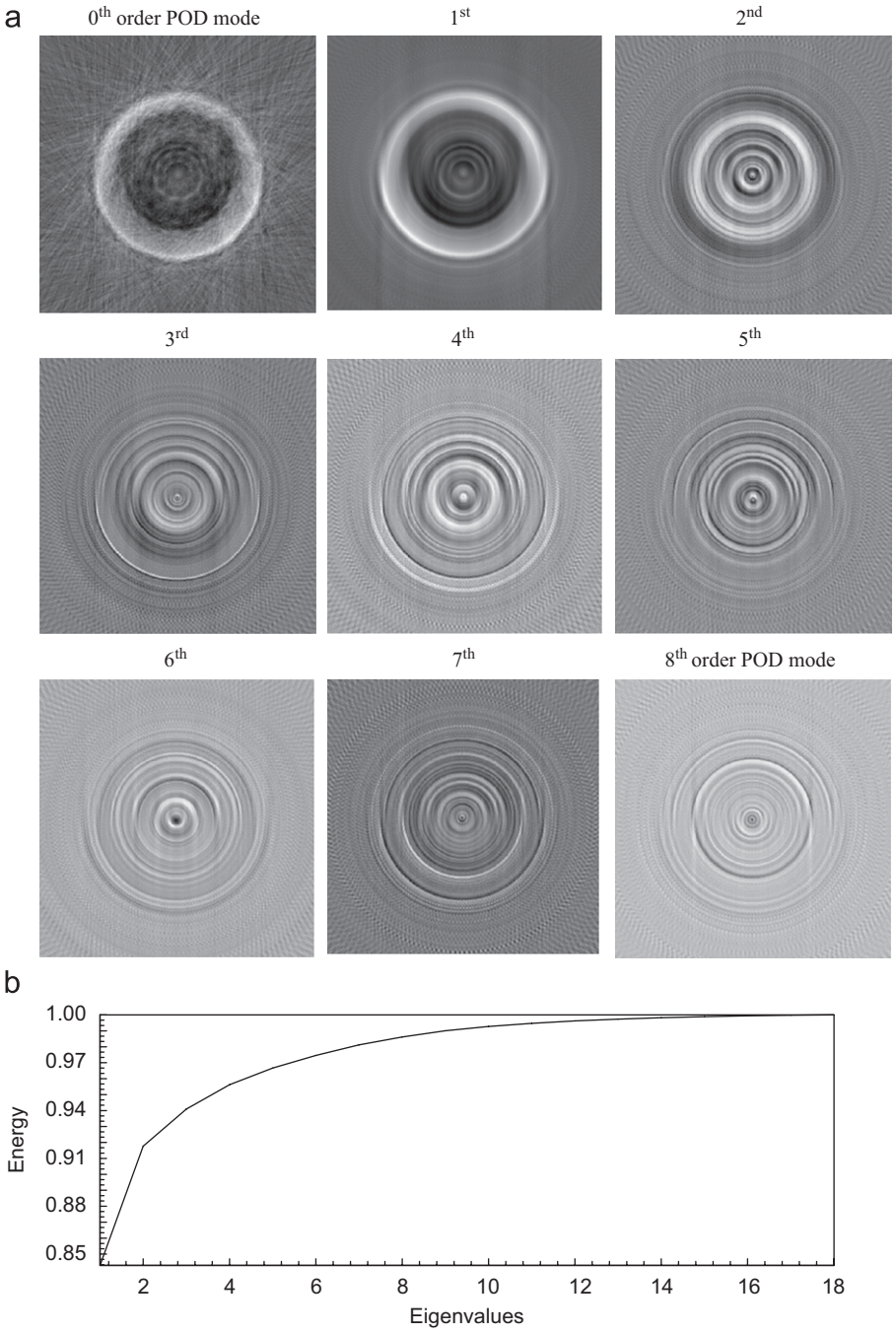

Fig. 6. (a) POD basis vectors (POD modes) of the reconstructed concentration gradients field at a horizontal plane (y/H=0.50) above the growing crystal and (b) variation of energies of the reconstructed POD basis modes with respect to their indices.

6.1. Reconstruction of two-dimensional modal images

The POD modes obtained after applying the algorithm of Section 2.3 are shown in Fig. 6. The images represent the two-dimensional distribution of modal contributions of the concentration gradients on a horizontal plane away from the growing crystal (y/H=0.50, H being the vertical extent of the schlieren image above the growing crystal). All modes show the appearance of concentric rings, indicating that the gradient field is practically axisymmetric. This symmetry is important from the view point of obtaining a proper crystal structure. Partial loss in symmetry and non-uniformity in the contour spacing, particularly in the core region can be attributed to the influence of crystal morphology which is closer to pyramidal than circular. Fig. 6(b) shows the variation of net energy content of the POD modes as a function of the mode index. It can be seen from the figure that the first 12 modes contribute 99% of the net energy and 18 of them contribute 99.9%. These are sufficient to capture the details of the time-dependent concentration field in the growth chamber. Remaining modes can be eliminated from further consideration, as they do not contribute substantially to the instantaneous concentration field.

To crosscheck the reconstruction procedure that combines principles of tomography and proper orthogonal decomposition, the following procedure has been followed. Reconstruction of the concentration gradients field has been performed at various time instants. The projection data is generated from the three-dimensional field by integration along the viewing direction. This step should yield the numerical equivalent of the schlieren image. A comparison of the reconstruction with the original experimental data is now possible. The comparison is shown in Fig. 7 for an intermediate horizontal plane (y/H=0.50) above the growing crystal in the growth chamber at three different time instants. An overall good match can be seen between the two data sets, thus validating the reconstruction scheme employed in the present work.

6.2. Reconstruction of time-dependent concentration gradient field

The rate of solute deposition onto the crystal faces can be directly correlated with the magnitude of the concentration gradients prevailing in the growth chamber. Hence, it is interesting to obtain a time history of the variation of concentration gradients in the crystal vicinity as well as in the regions away from the growing crystal. The three-dimensional modal analysis of the concentration gradients field can be extended to determine the time history of the concentration gradients field in the growth chamber by using the time components available after POD analysis. However, for this analysis to be meaningful, the time component of the projection data i.e. $u_k(t)$, k=1…N in Eq. (1) generated by POD analysis at different projection angles must be close. To verify this requirement in the context of the present work, the magnitude of the first four dominant modes with respect to time are plotted for three projection angles (in an interval of 45°) in Fig. 8(a). Though the time variation of the magnitude of the basis functions is not strictly identical for the four views, an approximately similar variation in qualitative terms exists for the three projection angles. In view of this observation, the following approach is suggested. Instead of multiplying the 2-D modes by the respective time components, the average of the time components available for all the projection angles has been utilized to reconstruct the time-dependent gradients field.

Following the above approximation, the reconstruction of the concentration gradients field at two horizontal planes closer to the crystal–solution interface (y/H=0.01 and 0.025) has been performed. Fig. 8(b) shows first four significant modes of the concentration gradients and the reconstructed gradient fields are shown in Fig. 8(c). One would expect a more pronounced role of the crystal morphology, which is closer to pyramidal rather than circular, in influencing the distribution of the concentration gradients near the crystal growth interface. This observation follows from the reconstructed concentration gradient field. Here, the data is not perfectly axisymmetric around the periphery, primarily due to the influence of the grown crystal surfaces and its edges on the orientation of the rising convection currents, though symmetry in high concentration gradients can be seen in the form of concentric rings (y/H=0.01) within the core region. The strength of these gradients gradually decreases as one moves away from the crystal as evident from the difference in the number of concentric rings (in the core region) seen for the planes y/H=0.01 and 0.025. Fluid convection affects the distribution of the concentration gradients in the regions near the crystal surface edges. However, overall symmetry is better restored as one moves towards the bulk of the solution (away from the crystal–solution interface, where the role played by the crystal morphology is quite negligible) as shown earlier in Fig. 6.

The variation of the concentration gradients in the growth chamber with time, especially near the crystal surface–solution interface can provide important information in addressing the coupled effects of fluid dynamics and mass transport that are often detrimental to the crystal quality. The rate of solute transport from the solution to the crystal surfaces is primarily controlled by the magnitude and orientation of concentration gradients in the crystal vicinity. Hence, larger the size of fluctuations of concentration gradients in time, higher would be

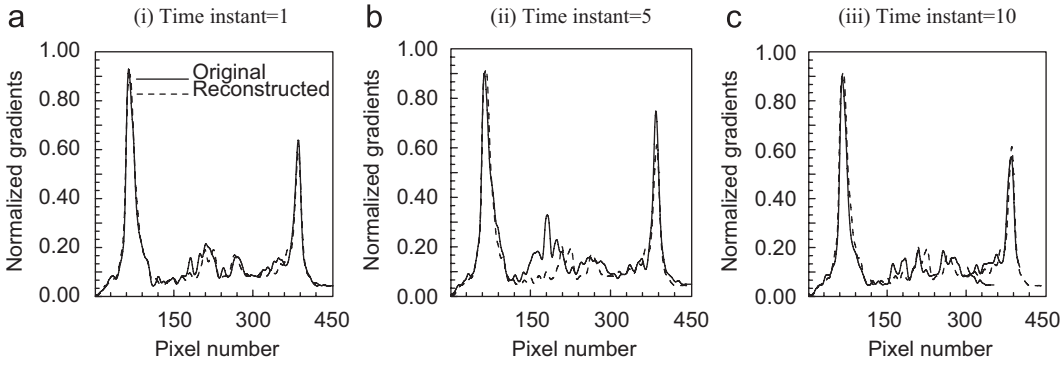

Fig. 7. Comparison of original and reconstructed concentration gradient profiles for a horizontal plane (y/H=0.50) above the growing crystal at three different time instants (1, 5 and 10).

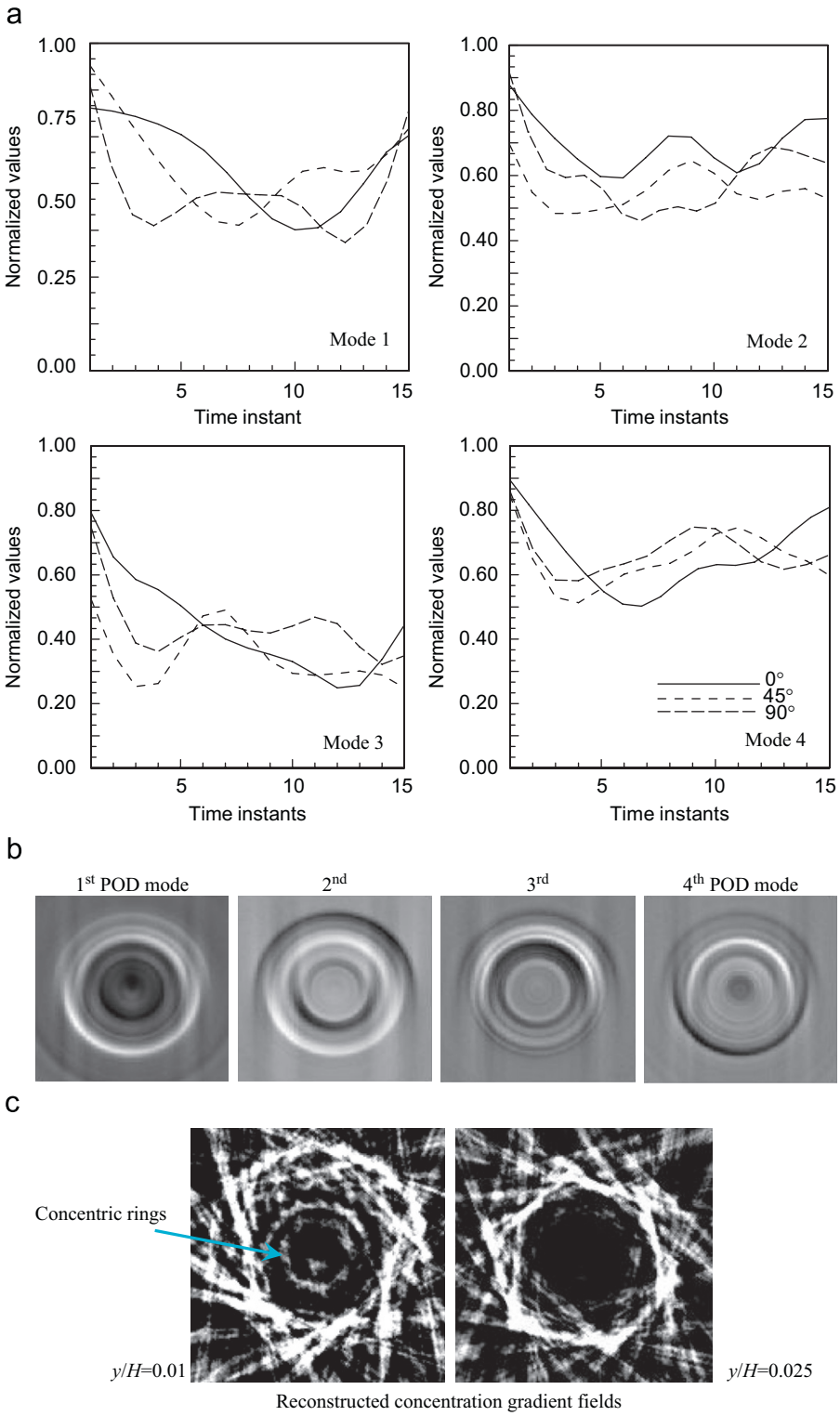

Fig. 8. (a) Variation of normalized modal values with respect to time for three projection angles (in an interval of 45°) for the first four dominant modes shown in (b); (c) reconstructed concentration gradient field at two horizontal planes near the crystal–solution interface (y/H=0.01 and 0.025).

the probability of the occurrence of morphological instabilities, such as macro steps, step bunches and solution inclusions on the growing crystal surfaces. The technique proposed in the present work is capable of analyzing how rapid these time variations are near the crystal–solution interface as well as in the regions away from the growing crystal. To demonstrate this capability, the temporal variations of the concentration gradients around the growing crystal over a period of 18 s have been reconstructed using the proposed technique and are shown in Fig. 9 for four horizontal planes (y/H=0.01, 0.025 (closer to the crystal–solution

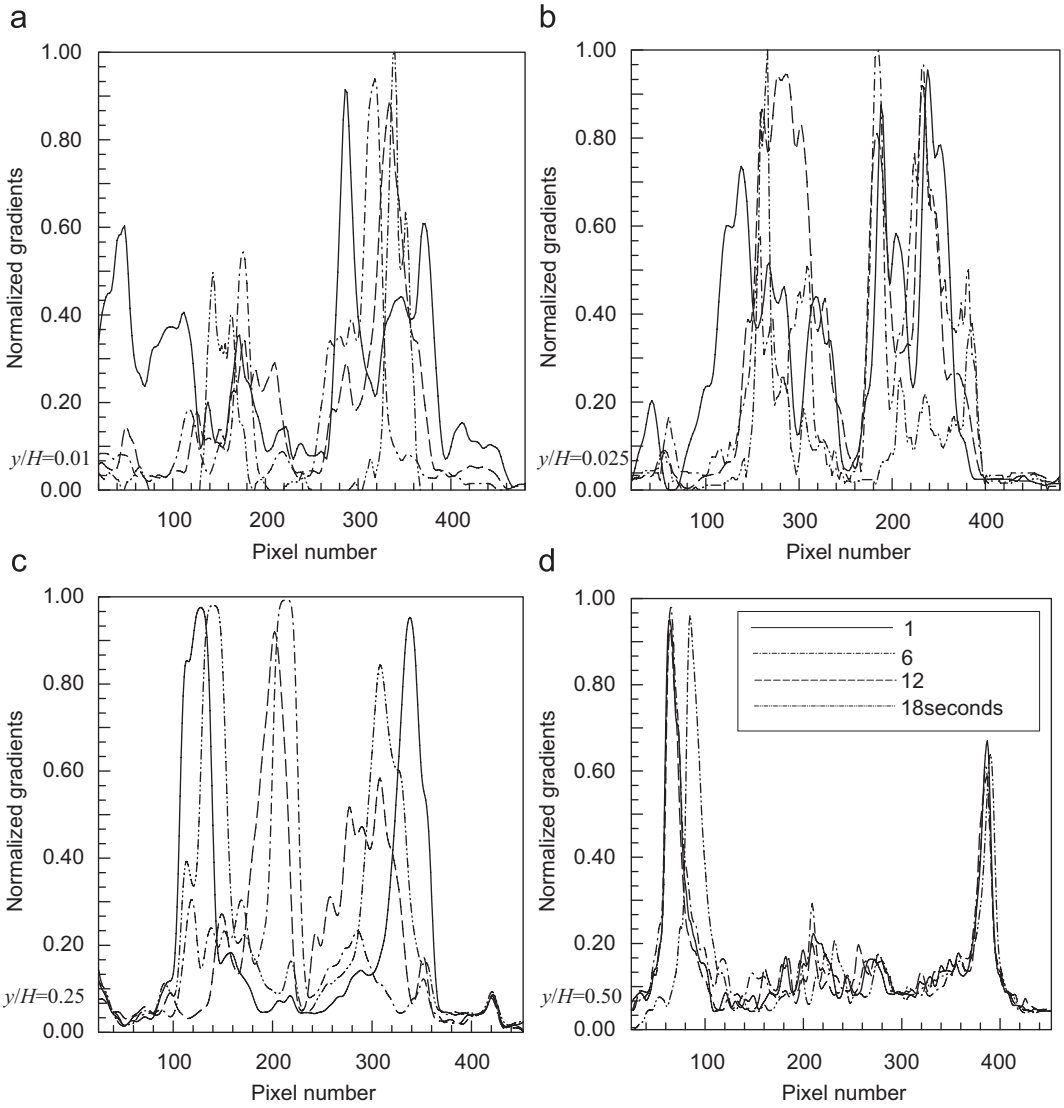

Fig. 9. Temporal variation of reconstructed concentration gradients at four horizontal planes (y/H=0.01, 0.025, 0.25 and 0.50) above the growing crystal over a period of 18 s. (y/H=0.0 corresponds to the top surface of the crystal). Large temporal fluctuations are to be seen for the planes closer to the crystal–solution interface (y/H=0.01, 0.025) compared to the bulk solution.

interface),[3] 0.25 and 0.50 (away from the growing crystal)). It is to be seen that in the vicinity of the crystal–solution interface, the concentration gradients and hence the rate of solute transport is purely time-dependent and relatively large temporal fluctuations at a given point along the horizontal plane can be seen in the plotted values. However, as one moves towards the bulk of the solution (y/H=0.25–0.50), the degree of unsteadiness decreases and a better symmetry is also to be seen in the temporal profiles. This can be attributed to the effect of crystal rotation which homogenizes the solution and orients the upward moving convection currents to follow a helical path as evident by two symmetrically located peaks (Fig. 7). These two peaks correspond to the path of the helical structure that rises symmetrically from the edges of the growing crystal. These are the regions of high concentration gradients indicated by bright intensity zones in the schlieren images. Hence, a practically axisymmetric and steady distribution of the gradient field on horizontal planes away from the crystal is confirmed. However, the gradients are strongly time-dependent near the crystal–solution interface and hence, the unsteadiness in the solute transport process is more pronounced in regions that are closer to the crystal surfaces.

7. Conclusions

A method based on combining proper orthogonal decomposition and computed tomography is proposed in the present work for the reconstruction of a time-dependent three-dimensional concentration gradient field. The potential of the proposed inversion scheme is demonstrated by reconstructing concentration gradients field on selected horizontal planes above a KDP crystal growing from its aqueous solution. The reconstruction

[3] How closely one can visualize the crystal–solution interface depends on the resolution of the imaging technique. The present work employs laser schlieren technique to visualize the concentration gradients around the growing crystal. One of the factors limiting the resolution of the laser schlieren technique is camera saturation at high intensities and it occurs in the regions of very high concentration gradients, which are close to the crystal–solution interface. This limitation can be overcome by employing more sensitive imaging techniques, e.g. interferometry and color schlieren, coupled with the proposed reconstruction algorithm to precisely address the growth conditions in these regions.

results of the concentration gradients field in the crystal growth chamber as obtained by the proposed scheme have been verified against the original experimental projection data. A satisfactory agreement was seen between the two data sets. The reconstructed two-dimensional POD modes reveal an overall axisymmetry of the concentration gradient field in qualitative terms. A slight loss of symmetry near the core region was also evident from the reconstructed spatial modes. The applicability of the proposed scheme is demonstrated by reconstructing the time history of concentration gradient field near the crystal–solution interface and in the regions away from the growing crystal. The results provide an insight into the distribution of concentration gradients near the crystal-solution interface and in the fluid. The reconstructed gradients field is found to be purely time-dependent in the crystal vicinity whereas the level of temporal fluctuations decreases towards the bulk of the solution. The effect of crystal morphology in the reconstructed gradient field near the crystal–solution interface is also revealed through reconstruction. The proposed algorithm provides for an extension of tomography principles to imaging unsteady processes that are often encountered in various processes of the crystal growth.

Acknowledgement

The authors thank Dr. Katsuo Tsukamoto, Professor, Department of Earth and Planetary Materials Science, Graduate School of Science, Tohoku University, Sendai, Japan for useful discussions and constructive suggestions during the revision of the manuscript.

References

[1] W.R. Wilcox, Prog. Cryst. Growth .Charact. 26 (1993) 153.
[2] M. Kawaji, O. Gamache, D.H. Hwang, N. Ichikawa, J.P. Viola, J. Sygusch, J. Crystal Growth 258 (2003) 420.
[3] K. Muralidhar, Atul Srivastava, P.K. Panigrahi, in: G.V. Karas (Ed.), New Topics in Crystal Growth Research, Nova Publishers, USA, 2005, pp. 1–126.
[4] R.J. Goldstein (Ed.), Fluid Mechanics Measurements, second ed., Taylor and Francis, New York, 1996.
[5] K. Onuma, T. Tsukamoto, S. Nakadate, J. Crystal Growth 129 (1993) 706.
[6] P.G. Vekilov, F. Rosenberger, J. Crystal Growth 186 (1998) 251.
[7] T. Inoue, K. Mori, Y. Kageyama, H. Mori, Cryst. Res. Technol. 35 (5) (2000) 587.
[8] F. Bedarida, L. Zefiro, P. Boccacci, J. Crystal Growth 61 (1983) 641.
[9] A.G. Notcovich, I. Braslavsky, S.G. Lipson, J. Crystal Growth 198–199 (1999) 10.
[10] Atul Srivastava, K. Muralidhar, P.K. Panigrahi, Appl. Opt. 44 (2005) 5381.
[11] M. Masayuki, M. Sugiyama, T. Ogawa, J. Crystal Growth 114 (1991) 71.
[12] E. Yokoyama, K. Okada, K. Tsukamoto, Forma 13 (1998) 363.
[13] L. Sirovich, M. Kirby, J. Opt. Soc. Am A 4 (3) (1987) 519.
[14] K. Fukanaga, Introduction to Statistical Pattern Recognition, Academic Press, New York, 1972.
[15] M.C. Romanowski, AIAA Paper 96-194, 1996.
[16] E.H. Dowell, K.C. Hall, J.P. Thomas, B.I. Epureanu, J. Heeg, AIAA Paper, 1999, p. 99.
[17] H.V. Ly, H.T. Tran, Proper orthogonal decomposition for flow calculations and optimal control in a horizontal CVD reactor, Center for Research in Scientific Computation, North Carolina State University, Technical report CRSC-TR98-12, 1998.
[18] P. Munshi, NDT & E Int. 25 (1992) 191.
[19] P. Munshi, NDT & E Int. 26 (1993) 235.
[20] F. Natterer, The Mathematics of Computerized Tomography, Wiley, New York, 1986.
[21] G.T. Herman, Image Reconstruction from Projections, Academic Press, New York, 1980.
[22] A. Srivastava, K. Muralidhar, P.K. Panigrahi, J. Crystal Growth 274 (2005) 191.
[23] A. Srivastava, K. Muralidhar, P.K. Panigrahi, J. Crystal Growth 267 (2004) 348.
[24] K. Nagashima, K. Tsukamoto, H. Satoh, H. Kobatake, P. Dold, J. Crystal Growth 293 (2006) 193.
[25] G.S. Settles, Schlieren and Shadowgraph Techniques: Visualizing Phenomena in Transport Media, Springer, New York, 2001.